https://doi.org/10.3311/PPch.43871

Periodica Polytechnica Chemical Engineering

Hydrothermal Cetyltrimethylammonium Bromide Modified Palm Oil Fuel Ash as a Mesostructured Silica-Based Adsorbent for Produced Water Treatment

Tutuk Djoko Kusworo[1*], Meitri Bella Puspa[1], Ahmad Fauzi Ismail[2], Andri Cahyo Kumoro[1]

[1] Department of Chemical Engineering, Faculty of Engineering, Diponegoro University, 13 Jl. Prof. Soedarto, 50275 Semarang, Central Java, Indonesia
[2] Advanced Membrane Technology Research Center (AMTEC), School of Chemical & Energy Engineering (SCEE), Faculty of Engineering, Universiti Teknologi Malaysia, Block N29a, 81310 Skudai Johor, Malaysia
* Corresponding author, e-mail: tdkusworo@che.undip.ac.id

Received: 03 March 2026, Accepted: 04 June 2026, Published online: 24 August 2026

Abstract

This study evaluates the adsorption performance of hydrothermally modified palm oil fuel ash (POFA) for the removal of chemical oxygen demand (COD) and ammonia nitrogen (NH_3–N) from produced water, while identifying the dominant equilibrium mechanisms governing pollutant uptake. The novelty of this work lies in the utilization of cetyltrimethylammonium bromide (CTAB)-assisted hydrothermal modification to enhance the mesostructural characteristics, surface functionality and adsorption selectivity of industrial POFA waste for simultaneous organic and nitrogen removal. Modified POFA was synthesized through hydrothermal treatment to improve surface reactivity, pore accessibility, and active site distribution. Adsorption experiments were conducted under varying contact times and adsorbent dosages to determine optimum operational conditions, while adsorption equilibrium behavior was analyzed using isotherm models. The results showed that the optimum contact time was 180 min and the optimum adsorbent dosage was 0.3 g. Under these conditions, COD removal reached 50.16 ± 1.03%, while NH_3–N removal achieved 49.66 ± 0.99%. At the optimum contact time, COD and NH_3–N removal efficiencies were approximately 53.98% and 38.34%. Isotherm analysis revealed that COD adsorption was best represented by combined Langmuir and Freundlich models (R^2 = 0.93), indicating adsorption on a partially heterogeneous surface involving both monolayer and multilayer interactions. In contrast, NH_3–N adsorption predominantly followed the Langmuir model (R^2 = 0.967). These findings demonstrate that mesostructured and surface-functionalized modified POFA exhibits distinct adsorption selectivity toward organic and nitrogenous pollutants, highlighting its potential as a sustainable adsorbent material for produced water treatment applications.

Keywords

POFA modification, adsorption, isotherm, pore structure optimization, produced water

1 Introduction

Produced water constitutes the predominant wastewater stream generated during upstream oil and gas operations, with its volume frequently exceeding that of the extracted hydrocarbons, particularly in mature reservoirs undergoing secondary and tertiary recovery. The effluent is characterized by a highly complex physicochemical composition, encompassing dispersed and dissolved petroleum hydrocarbons, polycyclic aromatic compounds, organic acids, production chemicals, heavy metals, and elevated concentrations of inorganic salts [1, 2]. This compositional heterogeneity results in high chemical oxygen demand (COD), oil and grease, total dissolved solids (TDS), and ionic strength, which collectively complicate treatment processes and challenge regulatory compliance [3]. Conventional treatment technologies including gravity separation, flotation, coagulation–flocculation, membrane filtration, and biological degradation often exhibit diminished performance under high salinity and in the presence of refractory organics [4]. In addition, limitations such as membrane fouling, secondary sludge generation, chemical-intensive operation, and reduced biodegradability frequently reduce treatment efficiency and increase operational complexity [5]. These challenges have driven increasing interest in adsorption-based treatment due to its operational simplicity,

Cite this article as: Kusworo, T. D., Bella Puspa, M., Ismail, A. F., Kumoro, A. C. "Hydrothermal Cetyltrimethylammonium Bromide Modified Palm Oil Fuel Ash as a Mesostructured Silica-Based Adsorbent for Produced Water Treatment", Periodica Polytechnica Chemical Engineering, 2026.
https://doi.org/10.3311/PPch.43871

high removal efficiency, and adaptability toward refractory contaminants [6, 7]. The adsorption performance is strongly influenced by the surface functionality, pore structure, and active site accessibility of the adsorbent material [8]. Therefore, the development of structurally robust mesostructured adsorbents derived from industrial waste materials has become an important strategy for improving the removal of organic and nitrogenous pollutants from produced water under harsh aqueous environments.

Concurrently, the transformation of agro-industrial residues into value-added functional materials represents a strategic direction in sustainable materials engineering [9]. Palm oil fuel ash (POFA), a byproduct of biomass combustion in palm oil mills, is generated in substantial quantities and is predominantly composed of silica-rich phases, largely in amorphous form [10]. The high silica content renders POFA a promising precursor for the synthesis of silica-based adsorbent. Nevertheless, pristine POFA typically exhibits low specific surface area, heterogeneous particle morphology, limited pore accessibility, and the presence of residual inorganic impurities [11]. These intrinsic structural constraints restrict their interfacial reactivity and adsorption efficiency, particularly in complex wastewater matrices such as produced water. Therefore, controlled structural modification is imperative to enhance its surface functionality and pore architecture.

Surfactant-assisted hydrothermal synthesis provides a rational approach to engineer mesostructured materials with tailored textural and chemical properties. Cetyltrimethylammonium bromide (CTAB), a cationic surfactant, functions as a structure-directing agent through electrostatic interactions between its positively charged ammonium head groups and negatively charged silanol species on silica surfaces [12]. Under hydrothermal conditions, CTAB micelle formation facilitates templated pore organization and surface reconstruction, enabling the development of more uniform mesoporosity and improved surface homogeneity [13]. The resulting mesoporous structure is particularly important for the adsorption of dissolved organic compounds and nitrogenous species because it provides accessible diffusion pathways and increases the availability of active adsorption sites. The larger pore channels facilitate the transport of COD related organic molecules and NH_3–N species into the internal surface of the adsorbent, thereby reducing diffusion resistance and improving adsorption efficiency. In addition, the silica framework derived from POFA plays an important role in maintaining structural stability and surface functionality during adsorption. The hydrothermal process promotes silica dissolution and reorganization, while CTAB directs the assembly of mesoporous silica domains through surfactant-templating mechanisms. This modification enhances surface reactivity by increasing exposed silanol groups and improving active site distribution on the adsorbent surface. Compared with conventional thermal activation or simple acid–base treatment, CTAB assisted hydrothermal modification allows for more precise control of pore size distribution and surface area while preserving the integrity of the silica framework [14]. The generation of a well-defined mesoporous network is particularly advantageous for adsorption applications in high-salinity wastewater systems, as it enhances mass transport, increases active site accessibility, and strengthens pollutant–surface interactions under diffusion-limited conditions [15]. Despite the increasing interest in utilizing POFA-derived silica materials for environmental remediation, studies specifically addressing the influence of CTAB assisted hydrothermal modification on the simultaneous adsorption of organic and nitrogenous pollutants remain limited. Previous investigations have predominantly focused on the application of POFA as a supplementary cementitious material [16], catalyst support [17], or general adsorbent [18], with limited attention given to the role of surfactant-assisted mesostructural engineering in controlling adsorption behavior toward COD related organic compounds and NH_3–N species in produced water systems. Furthermore, the relationship between CTAB directed pore formation, silica surface functionality, and adsorption performance toward different pollutant classes has not been comprehensively elucidated. Therefore, the present study aims to address this research gap by systematically investigating CTAB assisted hydrothermal modification influences the mesostructural characteristics, active site accessibility, and adsorption performance of POFA derived silica for the simultaneous removal of organic and nitrogenous contaminants from produced water.

The principal novelty of this study resides in the strategic integration of CTAB-mediated hydrothermal modification with biomass-derived POFA to construct a mesostructured silica-based adsorbent specifically designed for produced water treatment. The mesostructured framework is particularly important for this application because produced water contains complex contaminants, including dissolved organic compounds and nitrogenous species, which require accessible adsorption sites and efficient mass transfer pathways for effective removal. Through CTAB assisted pore formation, the modified POFA develops mesoporous channels and enhanced surface area that facilitate the diffusion and adsorption of COD related organic molecules and NH_3–N species. In addition, the mesostructure increases the

availability of exposed active sites while reducing diffusion resistance, thereby improving adsorption efficiency and interaction between pollutants and the adsorbent surface. While previous investigations have predominantly explored POFA as a supplementary cementitious material or low-cost adsorbent, the present work advances its functional role toward adsorption wastewater remediation through deliberate pore engineering and surface restructuring. Moreover, this research establishes a structure–performance correlation by systematically evaluating how mesostructural evolution influences adsorption behavior and adsorbent dosage-dependent efficiency in produced water matrices. This study aims to synthesize mesostructured silica derived from POFA *via* CTAB assisted hydrothermal modification, to comprehensively characterize the resulting structural and textural evolution, and to evaluate its adsorption performance, including the effect of adsorbent dosage in produced water treatment. Thereby elucidating the relationship between material properties and adsorption behavior.

2 Materials and methods

2.1 Materials

Palm oil fuel ash was used as the primary precursor and sieved to approximately 71 μm prior to modification. Citric acid (≥99%, Sigma-Aldrich, USA), sodium hydroxide (≥98%, Merck, Germany), and hydrochloric acid (37 wt%, Merck, Germany) were employed for acid–base pretreatment to remove impurities and enhance silica reactivity. Cetyltrimethylammonium bromide (CTAB, ≥99%, Sigma-Aldrich (Merck, Germany)) was used as a cationic structure-directing agent during hydrothermal synthesis. Deionized water (resistivity ≥18 MΩ·cm) was used for solution preparation and washing, while ethanol (≥96%) was applied for post-synthesis purification. All reagents were used without further purification.

2.2 Modification of palm oil fuel ash

POFA modification was carried out following the method reported by Hanifa et al. [17] as illustrated in Fig. 1. Initially, POFA was oven-dried at 100 °C for 24 h and sieved to obtain a uniform particle size of approximately 71 μm. To enhance its purity and reactivity, a sequential acid–base pretreatment was performed using citric acid, sodium hydroxide, and hydrochloric acid solutions. Subsequently, 25 g of POFA was dispersed in 150 mL solvent and stirred at 50 °C for 60 min. The mixture was filtered, and the solid residue was thoroughly washed with deionized water until neutral pH was achieved. The treated POFA was dried again at 100 °C for 24 h and calcined at 800 °C for 30 min.

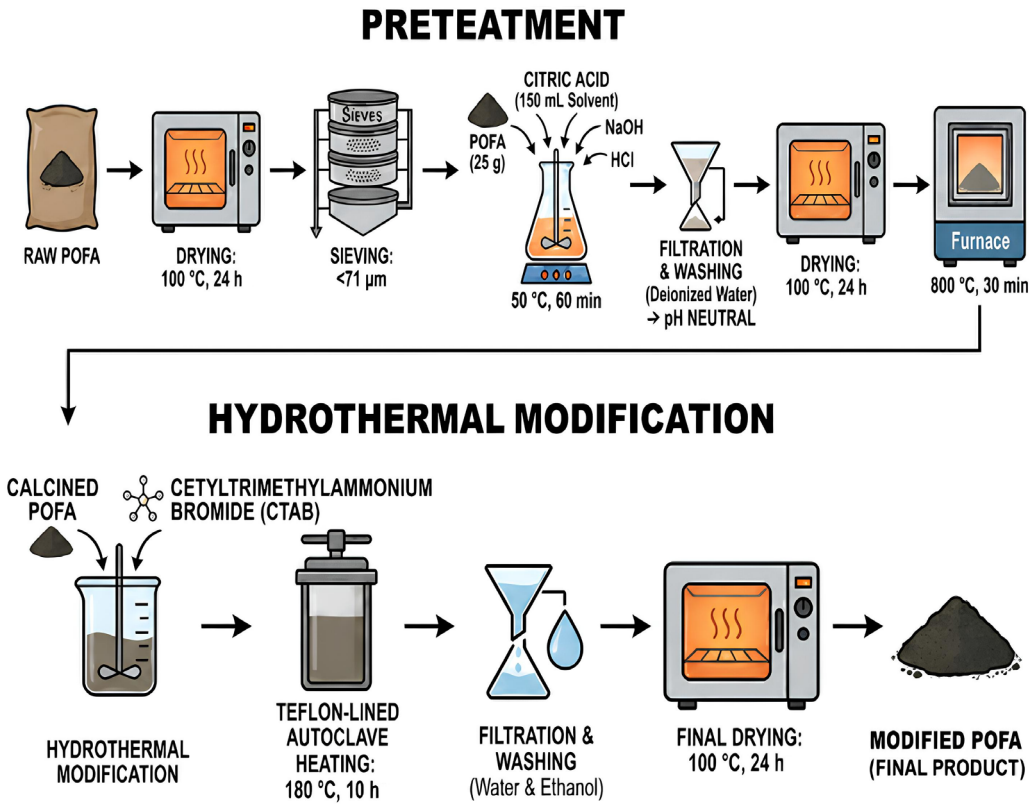

Fig. 1 Schematic representation of the POFA modification process

Hydrothermal modification was then conducted with the addition of CTAB as a structure-directing and pore-templating agent. The CTAB was first dissolved in deionized water under continuous stirring to ensure complete micelle formation before the addition of calcined POFA. The calcined POFA was then gradually introduced into the CTAB solution and continuously stirred to obtain a homogeneous suspension. The resulting mixture was transferred into a Teflon-lined stainless-steel autoclave and subjected to hydrothermal treatment at 180 °C for 10 h. During this process, CTAB functioned as a structure-directing and pore-templating agent, facilitating mesoporous silica formation and surface restructuring within the POFA matrix. After hydrothermal treatment, the product was allowed to cool naturally to room temperature, followed by filtration and repeated washing with deionized water and ethanol to remove residual surfactant species. The modified POFA was subsequently dried at 100 °C for 24 h prior to characterization and adsorption experiments.

2.3 Characterization of palm oil fuel ash

The surface morphology of POFA was examined using scanning electron microscopy (SEM) (JEOL JSM-LA Series, Japan), to evaluate particle shape, surface texture, and structural changes after modification. Elemental composition and spatial distribution were analyzed by SEM coupled with energy-dispersive X-ray spectroscopy (SEM–EDS), enabling both qualitative and quantitative assessment of major and minor elements. The chemical functionalities were characterized by Fourier-transform infrared (FTIR) spectroscopy (Thermo Fisher Scientific RaptIR instrument, USA). Surface textural properties, including specific surface area, pore volume, and pore size distribution, were determined using the Brunauer–Emmett–Teller (BET) method and the Barrett–Joyner–Halenda (BJH) model (Quantachrome Instruments, Switzerland) based on nitrogen adsorption–desorption isotherms.

2.4 Adsorption experiment

The adsorption behavior of POFA was evaluated using 100 mL aqueous samples under systematically varied operational parameters, including adsorbent dosage (0.1, 0.3, and 0.5 g), contact time (30–180 min), and temperature (30–75 °C). Following solid-liquid separation, the residual NH_3–N concentration in the supernatant was quantified using a UV-Vis spectrophotometer (Thermo Electron Scientific Instruments LLC., Madison, WI, USA). The corresponding removal efficiency and adsorption capacity were subsequently determined according to Eqs. (1) and (2):

$$R = \frac{C_0 - C_e}{C_0} 100\%, \tag{1}$$

$$Q_e = \frac{C_0 - C_e}{m} V, \tag{2}$$

where R (%) denotes removal efficiency, C_0 and C_e represent the initial and equilibrium pollutant concentrations, Q_e (mg/g) is the adsorption capacity, and m (g) and V (mL) correspond to the adsorbent mass and solution volume.

2.5 Adsorption isotherms

Adsorption isotherm analysis was conducted to elucidate the equilibrium relationship between the amount of pollutant adsorbed and its initial concentration on the adsorbent surface. The experimental data were fitted using linear Langmuir and Freundlich, Temkin, Dubinin–Radushkevich (D–R), Sips, Redlich–Peterson, and Fritz–Schlünder models, as expressed in Eqs. (3)–(10), respectively:

$$\frac{1}{Q_e} = \frac{1}{K_L Q_m C_e} + \frac{1}{Q_m}, \tag{3}$$

$$R_L = \frac{1}{1 + K_L C_0}, \tag{4}$$

$$\log Q_e = \log K_F + \frac{1}{n} \log C_e, \tag{5}$$

$$Q_e = \frac{RT}{b_T} \ln K_T + \frac{RT}{b_T} \ln C_e, \tag{6}$$

$$Q_e = q_m e^{-K\varepsilon^2}, \tag{7}$$

$$Q_e = \frac{Q_m K_s C_e^{m_s}}{1 + K_s C_e^{m_s}}, \tag{8}$$

$$Q_e = \frac{K_R C_e}{1 + a_R C_e^{\beta}}, \tag{9}$$

$$Q_e = \frac{K_{FS} C_e}{1 + a_{FS} C_e^{m_{FS}}}, \tag{10}$$

where Q_e and Q_m (mg/g) represent the equilibrium adsorption capacity and maximum adsorption capacity, respectively. C_0 and C_e (mg/L) denote the initial and equilibrium pollutant concentrations, respectively. K_L (L/mg) is the Langmuir constant related to adsorption affinity, while K_F and n are the Freundlich constants related to adsorption capacity and adsorption intensity, respectively. K_T and b_T represent the Temkin adsorption constant and Temkin constant related to adsorption heat, respectively. R is the universal gas constant (8.314 J/(mol·K)), and T is the absolute temperature (K). K_{DR} and β are the

D–R constants, where β is related to adsorption energy. ε represents the Polanyi potential. K_S and m are the Sips model constants related to adsorption capacity and heterogeneity, respectively. K_R, a_R, and β are the Redlich–Peterson model constants, while K_{FS}, a_{FS}, and m_{FS} are the Fritz–Schlünder model constants. R_L is the Langmuir separation factor, indicating the favorability of adsorption.

3 Results and discussion

3.1 Scanning electron microscopic surface analysis

The morphological characteristics of CTAB modified POFA were examined using scanning electron microscopy, as presented in Fig. 2 (a) and (b). At low magnification (×300), the material exhibits irregularly shaped particles with heterogeneous size distribution, forming aggregated clusters with rough and textured surfaces. This aggregative morphology suggests intensified interparticle interactions during the surfactant-assisted modification process [19]. The presence of CTAB as a structure-directing agent appears to influence surface assembly, promoting the formation of interconnected particulate networks rather than isolated grains [20]. At higher magnification (×1,000), the surface morphology becomes increasingly complex, characterized by protrusions, irregular flake-like structures, and microcrystalline domains dispersed across the particle surface. These features indicate that CTAB plays a significant role in regulating surface growth and reconstruction phenomena, thereby enhancing surface roughness [21]. The observed increase in surface roughness is functionally significant, as it enhances the effective surface area and elevates the density of accessible reactive sites. This morphological modification is likely to facilitate greater interfacial interactions between the active surface and target species, thereby potentially improving adsorption capacity.

The elemental composition and spatial distribution of CTAB modified POFA were further elucidated through EDS analysis, including the ternary compositional plot in Fig. 2 (d) and individual elemental mapping for Si, Ti, and O (Fig. 2 (e)–(g)). These results provide a more comprehensive understanding of the chemical uniformity and phase integration within the modified material. The Si–O–Ti ternary compositional plot shown in Fig. 2 (c) indicates that the majority of the data points are clustered within the

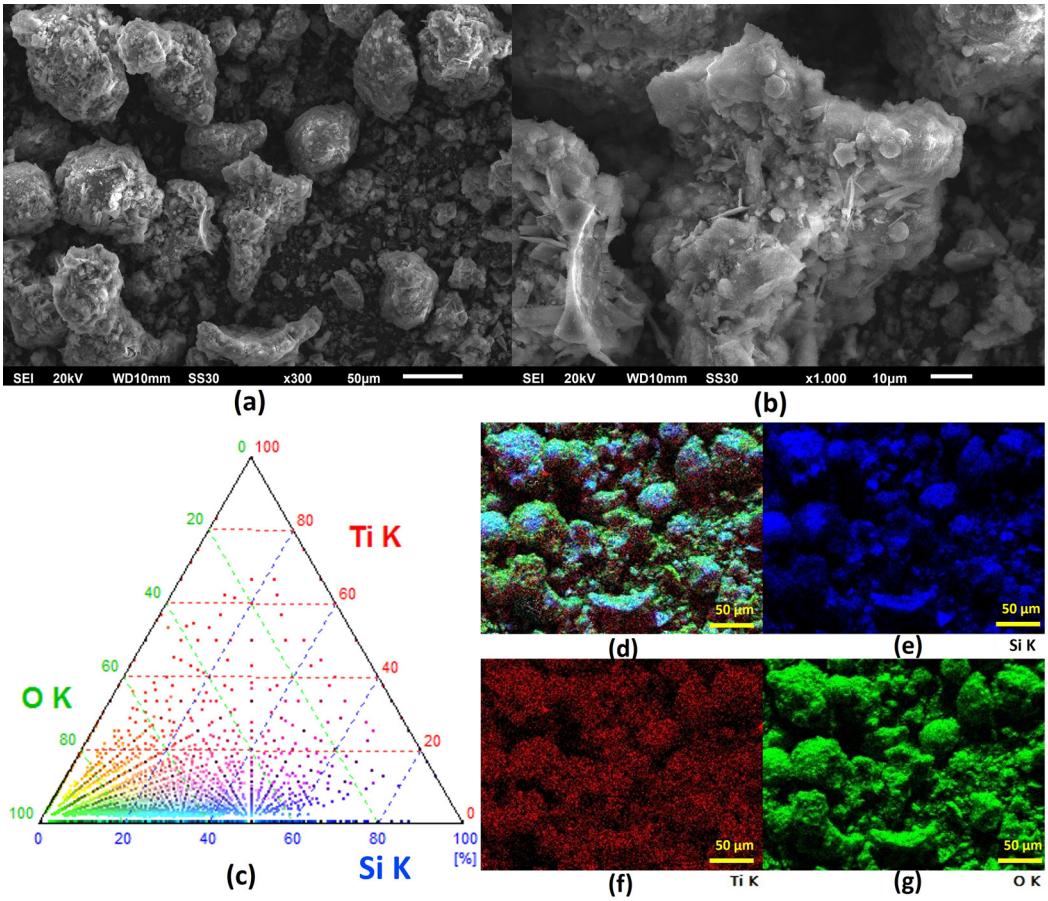

Fig. 2 SEM images of CTAB modified POFA at magnifications (a) ×300 and (b) ×1000; (c) Si–O–Ti ternary compositional plot; (d) overall EDS mapping, including element (e) Si, (f) Ti, and (g) O

oxygen- and silica-rich region, confirming that the structural backbone of the material is predominantly composed of SiO_2 based phases. The high oxygen fraction reflects the strong prevalence of metal-oxygen bonding environments, particularly Si–O–Si and Si–O–Ti linkages [22]. These oxygen-containing linkages play an important role in adsorption behavior by contributing to surface polarity, structural stability, and the availability of active adsorption sites. The Si–O–Si framework supports the formation of a stable mesoporous silica network that enhances surface area and facilitates the diffusion of organic and nitrogenous species into the internal pore structure [23]. The Si–O–Ti linkages contribute to enhanced surface reactivity and may promote stronger interactions between the adsorbent surface and pollutant molecules through electrostatic attraction and surface complexation mechanisms [24]. The Ti fraction, although comparatively lower is consistently distributed across the compositional domain rather than forming isolated Ti-rich vertices. This distribution pattern suggests that Ti species are not present as discrete segregated oxide domains but are instead integrated within the silica matrix. The absence of compositional drift toward a Ti-dominant region further supports the conclusion that CTAB assisted synthesis mitigates phase separation and promotes chemical homogeneity at the microscale [25]. The elemental mapping of Si in Fig. 2 (e) reveals an intense and continuous distribution across the entire particle surface, corroborating its role as the primary framework-forming element. The uniform Si signal without significant depletion zones indicates structural continuity of the silica network. This observation is consistent with the intrinsic composition of POFA, which is known to be rich in amorphous silica. Moreover, the spatial stability of Si suggests that the surfactant modification process does not disrupt the fundamental silicate backbone but rather modifies surface characteristics while preserving the bulk framework [17]. The Ti elemental map (Fig. 2 (f)) provides critical insight into the dispersion behavior of the titanium phase. The Ti signal appears homogeneously distributed over the silica surface without the presence of high-intensity localized clusters, which would otherwise indicate TiO_2 agglomeration. Such uniformity is particularly significant, as heterogeneous clustering could lead to reduced active site accessibility and compromised adsorption capacity. The even Ti dispersion implies strong interfacial interactions, potentially through the formation of Si–O–Ti bonds during synthesis or post-treatment. This interfacial bonding mechanism enhances phase compatibility and suppresses crystallite coalescence [26]. The role of CTAB in this context is likely associated with its function as a structure-directing and surface-stabilizing agent, where electrostatic interactions between the positively charged ammonium head groups and negatively charged silanol (S–OH) groups facilitate controlled nucleation and anchoring of Ti species [27]. The oxygen distribution map in Fig. 2 (g) exhibits an intense and spatially continuous signal, overlapping substantially with both Si and Ti regions. This overlap confirms that oxygen acts as the bridging element within the composite matrix, forming both Si–O–Si and Si–O–Ti networks. The uniform oxygen mapping further indicates that no oxygen-deficient domains are present, which would otherwise suggest incomplete oxide formation or structural defects. This homogeneous oxygen distribution supports the formation of a stable oxide lattice and reinforces the structural integrity of the composite. The ternary compositional analysis and elemental mapping demonstrate that CTAB assisted modification results in a chemically uniform Si–O–Ti system with effective titanium incorporation into a silica-dominated matrix. The absence of elemental segregation, the homogeneous Ti dispersion, and the consistent oxygen distribution collectively indicate the successful formation of an integrated composite architecture. Such structural uniformity is expected to enhance interfacial charge transfer, increase active site accessibility, and improve the overall physicochemical stability of the material in adsorption applications.

3.2 Chemical composition of modified palm oil fuel ash

The chemical composition of CTAB modified POFA was determined by EDS, as summarized in Table 1. The analysis

Table 1 Chemical composition analysis of modified POFA

Element	Mass (%)	Atom (%)	Compound	Mass (%)
C	33.13	71.71	C (element)	33.13
O	28.25			
Si	18.08	16.73	SiO_2	38.67
Na	3.23	1.83	Na_2O	4.36
Mg	2.19	2.34	MgO	3.63
Al	0.90	0.43	Al_2O_3	1.71
Ti	5.41	1.80	TiO_2	6.52
Ca	6.18	4.01	CaO	8.64
K	0.03	0.01	K_2O	0.04
Fe	1.17	0.54	FeO	1.50
Cu	1.44	0.16	CuO	1.81
Total	100.00	100.00		100.00

reveals that C, O, and Si are the predominant elements, with a relatively high carbon content (33.13 wt%). Although the POFA was calcined at 800 °C prior to modification, the detected carbon fraction may originate from residual mineral-associated carbon species that were not completely eliminated during thermal treatment, as well as carbon-containing surface species introduced through CTAB during the hydrothermal modification process. As CTAB functions as a structure-directing surfactant, partial retention or adsorption of surfactant-derived organic moieties within the developing mesoporous framework may occur even after washing. In addition, EDS is inherently surface-sensitive and provides semi-quantitative elemental information, which may overestimate the apparent carbon contribution due to surface-adsorbed species. Therefore, the detected carbon content should not be interpreted solely as residual bulk organic matter. Rather, it likely reflects a combination of minor residual carbonaceous phases and CTAB related organic species associated with the material surface. This interpretation is consistent with the molecular structure of CTAB as a long-chain alkyl ammonium surfactant, which can interact strongly with negatively charged silanol groups through electrostatic interactions, thereby stabilizing organic moieties on the silica surface. The retained carbonaceous and surfactant-derived surface functionalities are particularly relevant to adsorption applications because they may contribute to enhanced surface affinity and interfacial interactions with organic pollutants present in produced water. Silicon and oxygen constitute the primary components of the inorganic matrix, as confirmed by the presence of SiO_2 with a mass percentage of 38.67 wt%. The dominance of the silica phase suggests that the structural framework of the material remains chemically and thermally stable, providing a robust support for the dispersion of secondary metal oxides. This silica-rich framework is also essential for maintaining the mesostructural integrity generated during CTAB assisted hydrothermal treatment, thereby preserving pore accessibility and active adsorption sites required for pollutant diffusion and adsorption processes. In addition, the detection of alkali and alkaline earth oxides, including Na_2O, MgO, and CaO, reflects the inherent mineral complexity of POFA. These metal oxides may influence surface basicity and electrostatic interactions, which can affect the adsorption behavior of nitrogenous species such as NH_3–N.

Titanium is detected at 5.41 wt%, corresponding to 6.52 wt% TiO_2. This finding is consistent with the elemental mapping results, which indicate a relatively homogeneous distribution of Ti species across the particle surface. The absence of pronounced Ti-rich domains suggests effective dispersion without significant local agglomeration. Such homogeneous elemental distribution is important because it indicates that the CTAB assisted hydrothermal process successfully promoted chemical uniformity and minimized phase separation, which may contribute to more consistent adsorption activity across the adsorbent surface. Furthermore, minor metal oxides such as FeO and CuO, although present in low concentrations, may act as auxiliary active centers or contribute to modifications in the electronic structure of the composite system, potentially enhancing redox activity.

3.3 Fourier transform infrared sepctroscopic analysis

The FTIR spectrum of CTAB modified POFA demonstrates significant changes in surface functionality after the hydrothermal treatment process, indicating the successful incorporation of surfactant-assisted structural modification, as presented in Fig. 3. The dominant absorption band observed at approximately 1000–1100 cm^{-1} is attributed to the asymmetric stretching vibration of Si–O–Si bonds, confirming the presence of silica-based frameworks as the major constituent of POFA [28]. The intensity of this band suggests that the hydrothermal treatment preserved and reorganized the silicate network, which is essential for the formation of mesostructured adsorption sites. In addition, the band detected around 700–800 cm^{-1} corresponds to Si–O bending vibrations, further supporting the existence of silica-rich structures within the modified material.

A notable feature in the spectrum is the absorption band near 1450–1550 cm^{-1}, assigned to N–H bending vibrations.

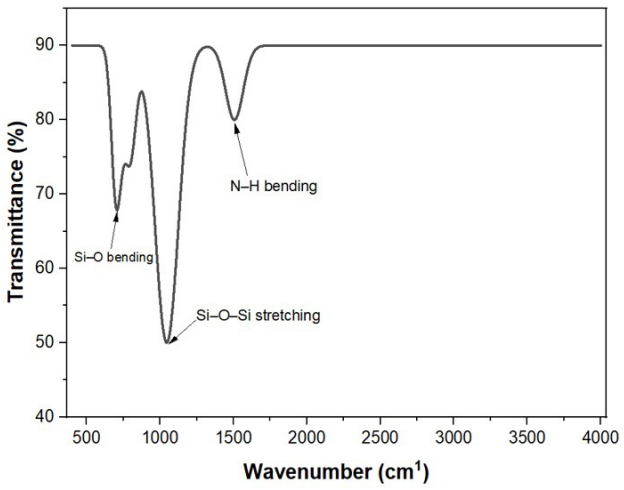

Fig. 3 FTIR spectrum of modified POFA

This band is associated with the presence of nitrogen-containing functional groups originating from cetyltrimethylammonium bromide. The appearance of this peak indicates that CTAB was not only utilized as a structure-directing agent during hydrothermal synthesis but also contributed to altering the surface chemistry of POFA [29]. This modification is closely related to the improvement of surface functionality, which refers to the presence and distribution of chemically active groups on the adsorbent surface that influence contaminant interaction and adsorption behavior. The incorporation or adsorption of CTAB-derived species onto the silica surface introduces polar and positively charged functional groups that can enhance electrostatic attraction toward dissolved contaminants, particularly ammonia-related species in produced water.

The role of CTAB is therefore significant in modifying the surface functionality and pore characteristics of POFA. During the hydrothermal process, CTAB molecules act as surfactant templates that guide the formation of more accessible mesoporous structures [30]. This templating effect improves pore distribution, increases surface heterogeneity, and enhances the exposure of adsorption-active sites. These structural and chemical modifications directly influence adsorption selectivity, which refers to the preferential adsorption behavior of the material toward specific pollutants depending on their physicochemical properties and adsorption mechanisms. Organic compounds contributing to COD are generally larger and relatively hydrophobic, favoring adsorption through van der Waals interactions and pore-filling mechanisms within the mesoporous silica framework. In contrast, NH_3–N species are smaller and their adsorption is more strongly governed by electrostatic interactions and the availability of polar surface functional groups.

The CTAB assisted hydrothermal treatment therefore improves the affinity of modified POFA toward both organic and nitrogen-containing pollutants by tailoring the surface chemistry and internal pore structure of the adsorbent. Furthermore, the mesostructured pore system generated during modification enhances contaminant diffusion and mass transfer into internal adsorption sites, thereby improving adsorption efficiency. The CTAB modified material exhibits improved surface heterogeneity and adsorption-active sites, which are beneficial for the simultaneous removal of organic pollutants and nitrogen-containing compounds. These FTIR findings support the adsorption results, confirming that the enhanced performance is directly related to the CTAB assisted hydrothermal modification rather than solely to the intrinsic composition of raw POFA.

3.4 Pore properties analysis

Surface textural properties were determined by low-temperature N_2 adsorption–desorption analysis. Prior to measurement, samples were degassed under vacuum to remove adsorbed species. The analysis was performed using a surface area and porosity analyzer, while the BET and BJH models were applied for post-experimental evaluation of specific surface area and pore size distribution, respectively, as summarized in Fig. 4 and Table 2. The POFA pure exhibited a relatively low specific surface area of 10 m^2/g, with a pore volume of 0.018 cm^3/g and an average pore diameter of 9.48 nm. The average pore diameter of 9.48 nm was calculated using the BJH method based on N_2 adsorption–desorption data, and derived from the relationship between total pore volume and BET surface area. These parameters indicate that untreated POFA is predominantly characterized by coarse mesoporous structures with limited pore accessibility, likely resulting from particle agglomeration and the presence of residual mineral phases partially obstructing pore channels [31]. Following modification, a significant enhancement in textural properties was observed. The specific surface area increased to 17 m^2/g, accompanied by a substantial rise in pore volume to 0.079 cm^3/g. This improvement suggests that the modification process effectively unblocked previously inaccessible pores and generated additional surface

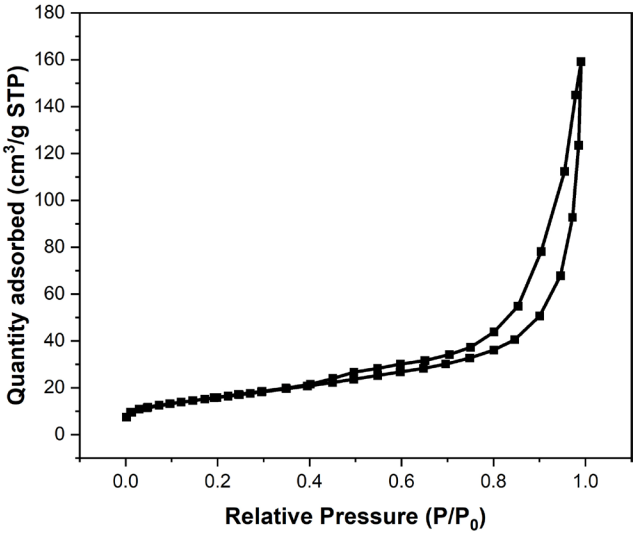

Fig. 4 Adsorption isotherm of modified POFA

Table 2 Pore properties of POFA

Sample	BET surface area (m^2/g)	Pore volume (cm^3/g)	Average pore size (nm)
POFA pure	10	0.018	9.48
POFA modification	17	0.079	2.87

exposure [32]. Concurrently, the average pore diameter decreased to 2.87 nm, indicating the formation of finer and more uniformly distributed mesopores. This reduction in pore size, coupled with increased pore volume, implies a pore restructuring mechanism in which irregular large pores in pristine POFA were reorganized or fragmented into smaller, more controlled mesoporous domains.

Fig. 4 exhibits a pronounced hysteresis loop within the intermediate-to-high relative pressure region which is characteristic of mesoporous materials according to the IUPAC physisorption isotherm classification. The presence of this hysteresis behavior indicates the occurrence of capillary condensation within mesoporous channels generated during the CTAB assisted hydrothermal modification process. The gradual increase in adsorption volume at intermediate relative pressures reflects the progressive filling of mesopores, whereas the sharp adsorption uptake when P/P_0 approaching unity is associated with condensation within larger mesoporous domains and interparticle voids. P/P_0 denotes the relative pressure in nitrogen physisorption, defined as the ratio of the equilibrium adsorbate pressure (P) to its saturation vapor pressure (P_0) at −196.15 °C. Furthermore, the non-overlapping adsorption–desorption branches suggest the existence of interconnected pore networks and restricted desorption pathways, which are commonly associated with complex mesostructured frameworks. These textural characteristics confirm that the CTAB assisted hydrothermal treatment successfully promoted the formation of a well-developed mesoporous silica architecture within the POFA matrix. The formation of this mesoporous framework plays a significant role in enhancing adsorption performance. The interconnected mesopore channels improve mass transfer and facilitate the diffusion of COD related organic compounds and NH_3–N species from the bulk solution into the internal adsorption sites. In addition, the increased pore accessibility and larger effective surface area contribute to a greater availability of active adsorption sites, thereby improving pollutant–surface interactions and adsorption efficiency. The mesostructural properties indicated by the hysteresis loop therefore provide important evidence that the CTAB modified POFA possesses favorable textural characteristics for adsorption applications in produced water treatment systems.

The BJH pore size distribution further corroborates the dominance of mesoporosity after modification, with a narrower and more defined distribution profile. The simultaneous decrease in average pore diameter and increase in total pore volume indicates the development of a more interconnected and accessible pore network. Such a structure is particularly advantageous for adsorption processes, as it provides a higher density of active sites while facilitating efficient mass transfer and pollutant diffusion into the adsorbent matrix [33]. Overall, the BET–BJH results demonstrate that the modification strategy effectively tailors the surface texture of POFA by enhancing specific surface area, enlarging pore volume, and refining pore size distribution toward a more homogeneous mesoporous regime. These structural improvements directly contribute to the enhanced adsorption performance of modified POFA, as reflected in kinetic, isotherm, and thermodynamic evaluations, underscoring the critical role of pore engineering in optimizing biomass ash-based adsorbents.

3.5 Effect of adsorbent dosage on produced water removal efficiency

The adsorption performance toward produced water contaminants is markedly influenced by adsorbent composition and dosage, as these parameters determine the availability of active surface sites, pore accessibility, and overall adsorption capacity [34]. In this study, the enhanced adsorption behavior is directly associated with the hydrothermal CTAB modification of POFA, which promotes the development of mesostructured silica surfaces, increases pore accessibility, and introduces a more favorable surface environment for contaminant interaction compared with raw POFA. The incorporation of CTAB during hydrothermal treatment contributes to the formation of surfactant-templated porous structures that improve adsorption site distribution and facilitate mass transfer during the adsorption process. As shown in Fig. 5 (a), both COD and NH_3–N removal efficiencies increase progressively with contact time from 30 to 180 min. The continuous rise in removal efficiency indicates that the adsorption process proceeds gradually toward equilibrium, with no abrupt saturation observed within the investigated time frame [35]. The highest removal efficiencies are achieved at 180 min, which is therefore identified as the optimum contact time under the present experimental conditions. At this duration, COD removal reaches approximately 42.51–53.98%, while NH_3–N removal approaches 30.32–38.34%, suggesting that the majority of accessible adsorption sites have been effectively utilized. The time-dependent behavior reflects the classical adsorption mechanism involving an initial rapid uptake phase followed by a slower approach to equilibrium. During the early stage (30–60 min), adsorption is primarily controlled by

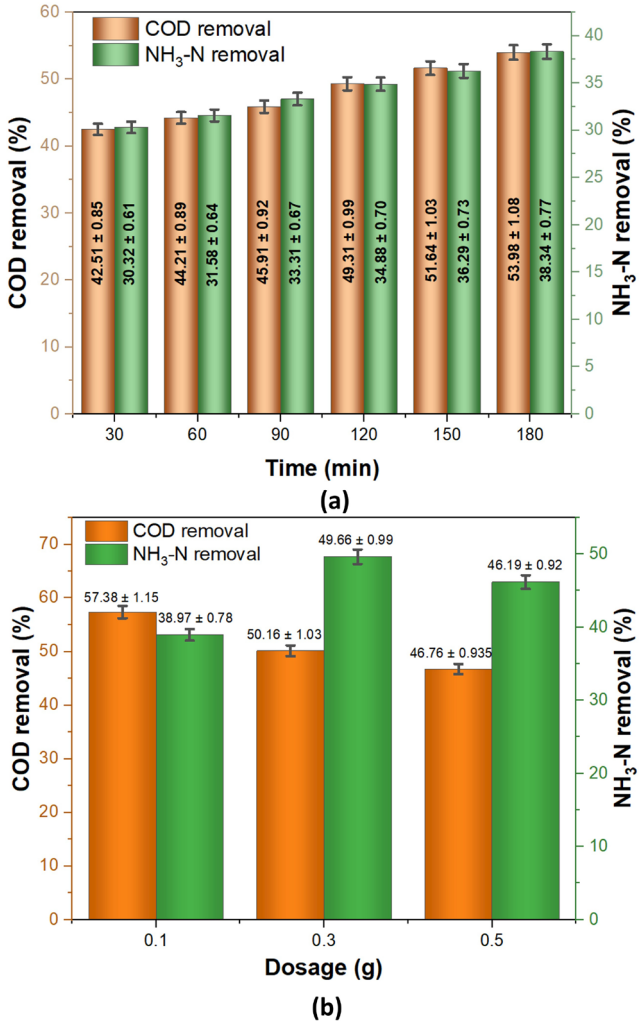

Fig. 5 Effect of operating parameters on COD and NH_3–N removal: (a) Contact time effect; (b) Dosage effect

external surface interactions driven by a high concentration gradient between the bulk solution and the adsorbent surface [36]. As time progresses, intraparticle diffusion becomes increasingly significant, governing the transport of solutes into internal pore structures. Beyond 120 min, the reduction in the driving force (Ci–Ce) and progressive occupation of active sites leads to a diminished adsorption rate, indicating that the system approaches equilibrium conditions.

Fig. 5 (b) presents the effect of adsorbent dosage on the removal efficiencies of COD and NH_3–N. At a dosage of 0.1 g, COD removal was 57.38 ± 1.15%, while NH_3–N removal reached 38.97 ± 0.78%. Increasing the dosage to 0.3 g resulted in a marked improvement in NH_3–N removal, achieving 49.66 ± 0.99%, whereas COD removal slightly decreased to 50.16 ± 1.03%. At the highest tested dosage of 0.5 g, COD and NH_3–N removal efficiencies were 46.76 ± 0.935% and 46.19 ± 0.92%, respectively. These results indicate that increasing the adsorbent dosage enhances the total number of available active sites. However, COD removal efficiency is comparatively higher at the lowest dosage of 0.1 g. This phenomenon can be attributed to the more effective utilization of adsorption sites at low adsorbent concentrations. At higher dosages, particle aggregation and overlapping of active sites reduce the effective surface area accessible for adsorption and impede mass transfer processes. Consequently, COD removal exhibits a slight decline as the adsorbent loading increases. The improvement in NH_3–N removal at 0.3 g is associated with the increased availability of adsorption sites, which facilitates stronger interactions between the adsorbent surface and nitrogen species. This enhanced interaction is also related to the CTAB assisted hydrothermal modification, which improves surface functionality and mesoporosity, thereby increasing the accessibility of adsorption sites for ammonia-containing species. At a dosage of 0.5 g, both COD and NH_3–N removal efficiencies decline relative to the 0.3 g condition. This reduction is primarily due to the aggregation of adsorbent particles and the consequent overlapping of active sites, which limit the effective surface area available for solute interaction. In addition, high solid concentrations can impair mixing efficiency and introduce diffusional limitations within the suspension, thereby restricting mass transfer and adsorption kinetics. Despite the theoretical increase in total adsorption sites, these physical constraints diminish the per-unit adsorption performance. Therefore, the 0.5 g dosage is considered suboptimal, as it does not enhance removal efficiency and may pose operational challenges, including increased sludge production and handling complexity. Overall, the optimal adsorbent dosage is identified as 0.3 g, which provides a balance between maximizing active site availability for NH_3–N adsorption and minimizing aggregation effects that adversely affect COD removal. These findings highlight the critical importance of adsorbent dosage optimization in achieving efficient simultaneous removal of organic and nitrogenous pollutants.

The distinct removal trends between COD and NH_3–N indicate differences in adsorption affinity and mechanism. Organic constituents contributing to COD are generally larger and more hydrophobic, favoring surface adsorption *via* van der Waals interactions and pore filling [37, 38]. In contrast, ammonia species are smaller and their adsorption is more strongly influenced by electrostatic interactions and the presence of specific surface functional

groups [39]. Therefore, adsorbent composition, particularly its surface chemistry and pore structure distribution, plays a crucial role in determining the adsorption efficiency and selectivity toward different pollutants.

3.6 Adsorption isotherms: Langmuir, Freundlich, Temkin, Dubinin–Radushkevich, Sips, Redlich–Peterson, and Fritz–Schlünder

The adsorption behavior of COD and NH_3–N onto modified POFA was systematically evaluated using multiple isotherm models, including Langmuir, Freundlich, Temkin, D–R, Sips, Redlich–Peterson, and Fritz–Schlünder (Figs. 6 and 7), in order to obtain a comprehensive understanding of the adsorbate-adsorbent interaction mechanisms as summarized in Tables 3 and 4. This multi-model approach enables differentiation between homogeneous and heterogeneous surface assumptions, as well as between monolayer, multilayer, and pore-filling adsorption mechanisms.

For COD adsorption, the Langmuir model exhibited strong agreement with the experimental data (R^2 = 0.92765), suggesting that adsorption predominantly occurs *via* monolayer coverage on energetically uniform active sites. The remarkably high maximum adsorption capacity (Q_m = 755.49 mg/g) highlights the substantial potential of modified POFA for the removal of complex organic constituents. The relatively low Langmuir constant (K_L = 0.00055 L/mg) indicates that although the adsorption capacity is high, the affinity constant is moderate, reflecting a gradual occupation of active sites [40, 41]. This behavior is consistent with the heterogeneous nature of COD, which comprises a broad spectrum of organic molecules with varying molecular sizes, polarities, and functional groups.

The Freundlich model also demonstrated comparable goodness of fit (R^2 = 0.92790), with an n^{-1} value close to unity (1.03219), indicating moderate surface heterogeneity. This suggests that the modified POFA surface does not consist of perfectly uniform adsorption sites but instead contains a distribution of energetically diverse sites arising from silanol groups, minor metal oxides, and residual carbonaceous phases [42]. The adequacy of the Freundlich model confirms that COD adsorption is not exclusively governed by a single monolayer mechanism but likely involves multilayer adsorption on a heterogeneous surface.

MAPE (mean absolute percentage error) represents the average percentage deviation between the experimental observations and the predicted values, while RMSE (root mean square error) provides a measure of the overall prediction error by calculating the square root of the mean squared residuals.

The adsorption energy (E) in the Dubinin–Radushkevich model was calculated from the D–R constant (β) using $E = \left(1/\sqrt{2\beta}\right)$, where β is obtained from the linear plot of $\ln(q_e)$ versus ε^2. The obtained value of E = 50.83 kJ/mol indicates strong adsorbate–adsorbent interactions, suggesting a chemisorption-dominated mechanism. The Temkin model provided slightly lower correlation (R^2 = 0.91438); however, the Temkin constant (b_T = 127.31 J/mol) reveals that adsorption energy decreases progressively with increasing surface coverage. This indicates the presence of adsorbate–adsorbate interactions, where repulsive forces between adsorbed organic molecules reduce the heat of adsorption as surface occupancy increases. Such behavior is typical for complex organic mixtures where molecular crowding influences adsorption thermodynamics [43].

Although the D–R model exhibited lower correlation (R^2 = 0.88499), the calculated mean adsorption energy (E = 50.83 kJ/mol) is significantly higher than the threshold commonly associated with physical adsorption (<8 kJ/mol). This high energy value strongly suggests that COD adsorption is dominated by chemisorption mechanisms involving surface complexation or specific chemical bonding rather than weak van der Waals interactions [44]. The predominance of chemisorption is consistent with the presence of reactive functional groups on modified POFA capable of interacting strongly with oxygenated and aromatic organic compounds.

Hybrid models such as Sips, Redlich–Peterson, and Fritz–Schlünder yielded correlation coefficients comparable to those of Langmuir and Freundlich ($R^2 \approx 0.928$), indicating that COD adsorption behavior lies within a transitional regime between ideal homogeneous and heterogeneous systems. The comparable performance of these models supports the interpretation that COD adsorption involves a combination of monolayer coverage and multilayer interactions on a surface exhibiting partial heterogeneity [45].

The adsorption isotherm analysis for NH_3–N was evaluated using classical and hybrid isotherm models to better understand the adsorption mechanism of CTAB modified POFA. Among the investigated models, the Langmuir model exhibited the best overall fitting performance, with the highest correlation coefficient (R^2 = 0.967) together with very low error values ($\chi^2 = 3.567 \times 10^{-7}$, RMSE = 0.138, and MAPE = 0.002). The χ^2 value (3.567×10^{-7}) represents the normalized squared deviation between the experimental data and the model predictions, where the extremely low magnitude indicates a negligible discrepancy and a high degree of agreement. The RMSE (0.138) quantifies the standard deviation of prediction errors, reflecting

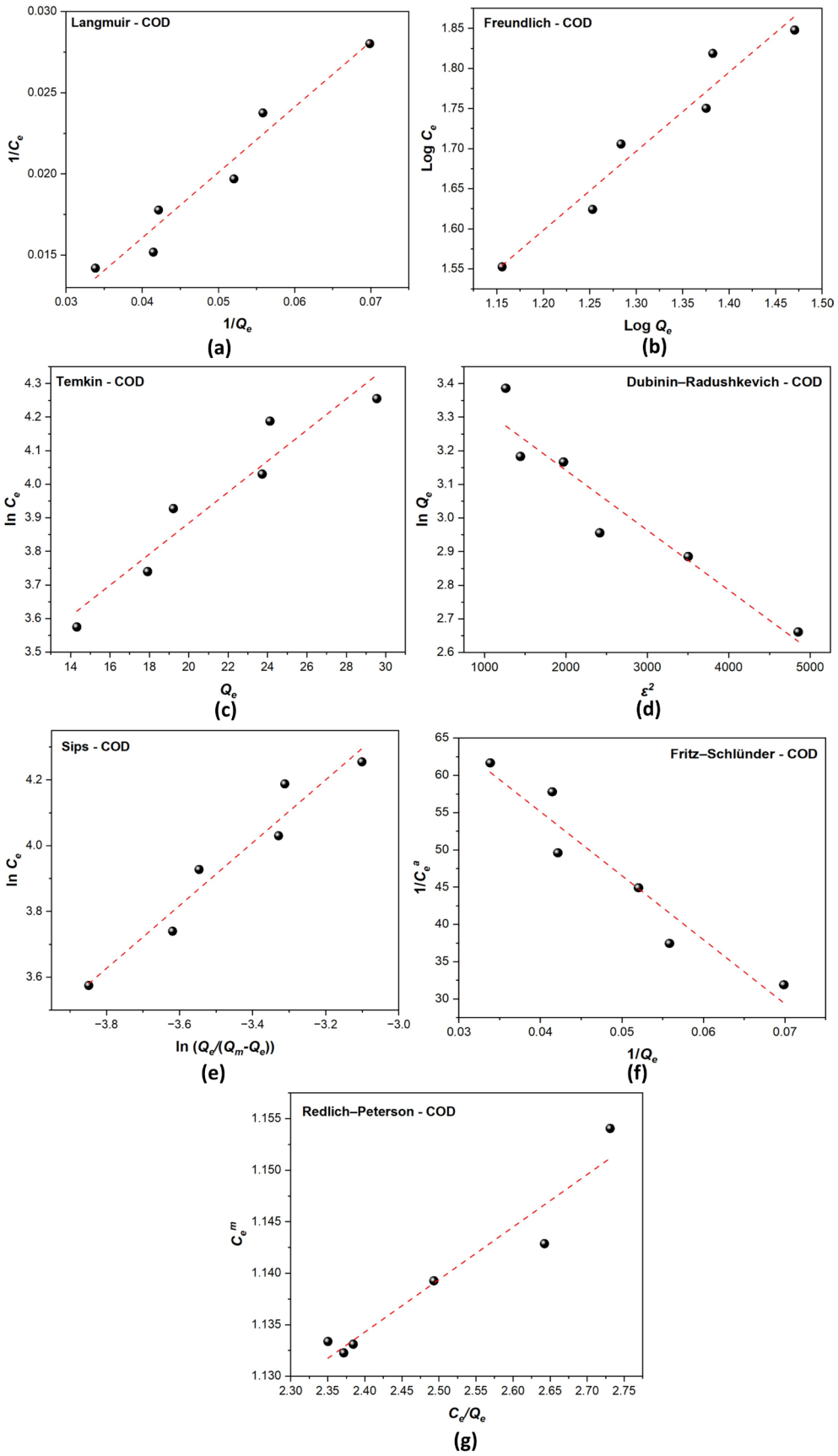

Fig. 6 Linearized adsorption isotherm models for COD removal: (a) Langmuir; (b)Freundlich; (c) Temkin; (d) Dubinin–Radushkevich; (e) Sips; (f) Redlich–Peterson; (g) Fritz–Schlünder models

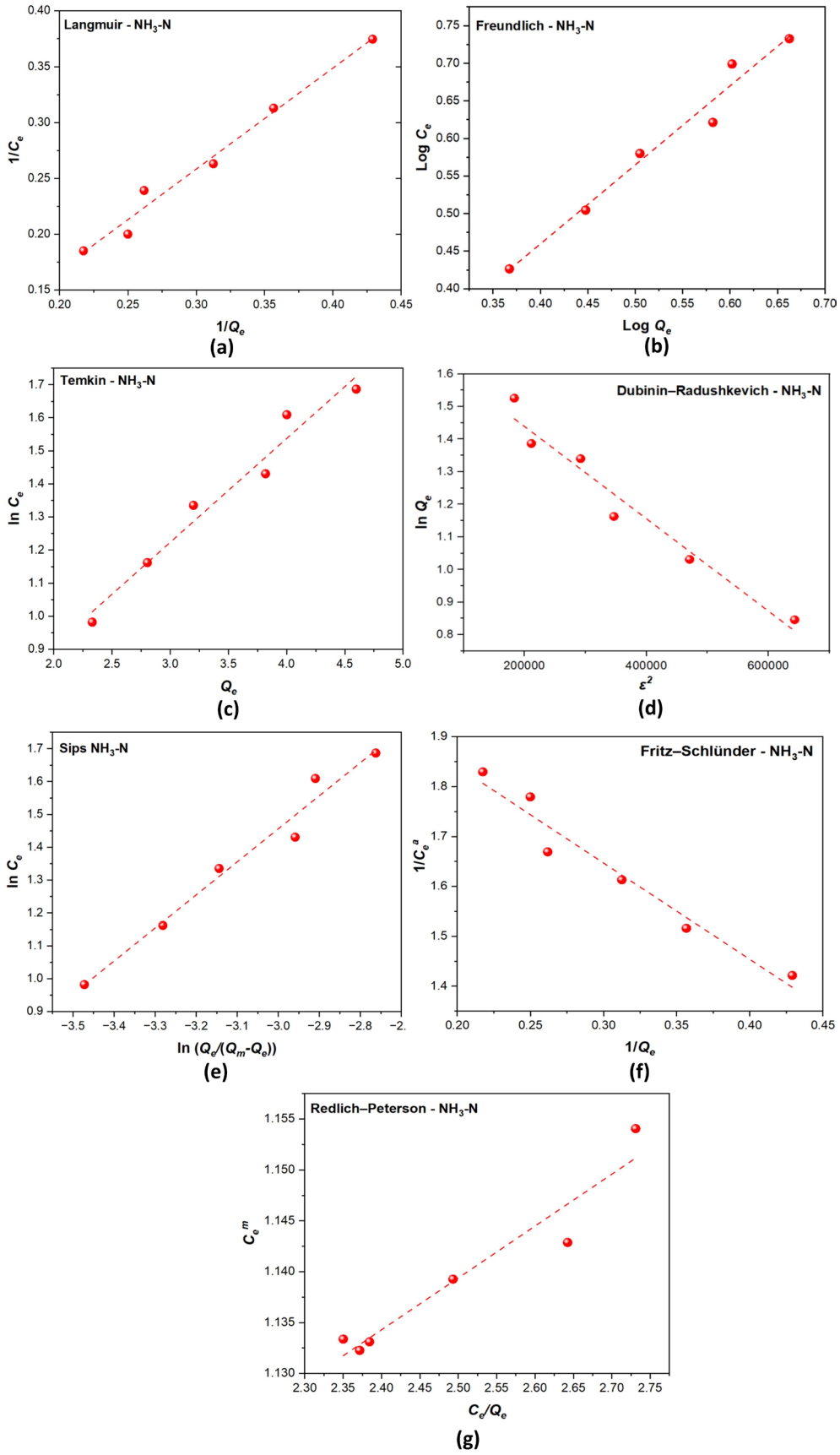

Fig. 7 Linearized adsorption isotherm models for NH_3–N removal: (a) Langmuir; (b)Freundlich; (c) Temkin; (d) Dubinin–Radushkevich; (e) Sips; (f) Redlich–Peterson; (g) Fritz–Schlünder models

Table 3 Isotherm model parameters for modified POFA at COD adsorption

Isotherm models	Parameters	POFA modified
Langmuir	Q_m (mg/g)	755.488
	K_L (L/mg)	0.001
	R^2	0.928
	χ^2	0.001
	RMSE	1.328
	MAPE	0.009
Freundlich	K_F	0.454
	n^{-1}	1.032
	R^2	0.928
	χ^2	4.345 E-06
	RMSE	1.326
	MAPE	0.003
Temkin	b_T (J/mol)	127.312
	K_T (L/mg)	0.057
	R^2	0.914
	χ^2	3.773 E-09
	RMSE	1.445
	MAPE	0.001
Dubinin-Radushkevich	Q_m (mg/g)	34.344
	K_D (mol/kJ)^2	0.001
	E (kJ/mol)	50.826
	R^2	0.885
	χ^2	0.001
	RMSE	1.675
	MAPE	0.016
Sips	Q_m (mmol/g)	685.931
	N	2.648
	K_s (mL/mol)	0.001
	R^2	0.928
	χ^2	0.001
	RMSE	1.329
	MAPE	0.003
Redlich-Peterson	K	4.078
	n	0.034
	a	7.984
	R^2	0.928
	χ^2	4.813 E-06
	RMSE	1.326
	MAPE	0.003
Fritz–Schlünder	K_1	0.455
	b	0.085
	K_2	0.003
	a	0.969
	R^2	0.928
	χ^2	4.372 E-06
	RMSE	1.326
	MAPE	0.003

Table 4 Isotherm model parameters for modified POFA at NH_3–N adsorption

Isotherm models	Parameters	POFA modified
Langmuir	Q_m (mg/g)	39.271
	K_L (L/mg)	0.024
	R^2	0.967
	χ^2	3.567 E-07
	RMSE	0.138
	MAPE	0.002
Freundlich	K_F	0.968
	n^{-1}	1.095
	R^2	0.966
	χ^2	6.507 E-07
	RMSE	0.139
	MAPE	0.003
Temkin	b_T (J/mol)	819.635
	K_T (L/mg)	0.784
	R^2	0.965
	χ^2	2.362 E-09
	RMSE	0.143
	MAPE	0.001
Dubinin-Radushkevich	Q_m (mg/g)	3.109
	K_D (mol/kJ)^2	0.004
	E (kJ/mol)	59.199
	R^2	0.754
	χ^2	0.235
	RMSE	0.839
	MAPE	1.871
Sips	Q_m (mmol/g)	77.414
	N	0.369
	K_s (mL/mol)	0.002
	R^2	0.874
	χ^2	2.989
	RMSE	1.224
	MAPE	7.639
Redlich-Peterson	K	0.902
	n	1.626
	a	0.052
	R^2	0.916
	χ^2	2.962
	RMSE	1.192
	MAPE	7.596
Fritz–Schlünder	K_1	1.448
	b	0.085
	K_2	0.003
	a	0.358
	R^2	0.918
	χ^2	2.992
	RMSE	1.223
	MAPE	7.643

the absolute average deviation between experimental and calculated values; lower RMSE values correspond to improved model accuracy. Meanwhile, the MAPE (0.002) expresses the average absolute percentage error relative to the experimental data, with values approaching zero indicating excellent predictive performance and minimal relative deviation. The excellent agreement between experimental and predicted adsorption data suggests that NH_3–N adsorption predominantly occurs through monolayer adsorption on relatively homogeneous active sites distributed over the adsorbent surface. The Langmuir maximum adsorption capacity Q_m of 39.271 mg/g further demonstrates the favorable adsorption affinity of the CTAB modified POFA toward ammonia-containing species. This behavior indicates that the hydrothermal CTAB modification successfully generated accessible adsorption-active sites with relatively uniform adsorption energy.

The Freundlich model also demonstrated a strong fitting performance, with $R^2 = 0.966$ and low statistical error values (RMSE = 0.139 and MAPE = 0.003). The close agreement between Langmuir and Freundlich fitting results suggests that although the adsorption surface exhibits a certain degree of heterogeneity, the adsorption process is still dominated by energetically favorable surface interactions. The Freundlich constant ($K_F = 0.968$) and adsorption intensity parameter ($n^{-1} = 1.095$) indicate that NH_3–N adsorption occurs favorably on the modified POFA surface. The slight surface heterogeneity implied by the Freundlich model may originate from the mesostructured silica framework and the distribution of CTAB derived functional groups formed during hydrothermal treatment.

Similarly, the Temkin model provided an excellent fit to the experimental data, with $R^2 = 0.965$ and the lowest χ^2 value among all models (2.362×10^{-9}), indicating strong consistency between theoretical assumptions and experimental adsorption behavior. The Temkin constant ($b_T = 819.635$ J/mol) suggests that significant adsorbate–adsorbent interactions occur during NH_3–N adsorption. Unlike the Langmuir model, the Temkin model considers the effect of indirect adsorbate interactions and assumes that the heat of adsorption gradually decreases with increasing surface coverage. Therefore, the good fitting performance indicates that electrostatic interactions and surface interaction energies play an important role in controlling NH_3–N adsorption on CTAB modified POFA. This finding is consistent with the FTIR analysis, which confirmed the presence of CTAB-derived polar functional groups capable of enhancing adsorption affinity toward nitrogen-containing species.

In contrast, the D–R model exhibited substantially poorer fitting performance, with a lower correlation coefficient ($R^2 = 0.754$) and significantly higher error values (RMSE = 0.839 and MAPE = 1.871). The D–R model is commonly associated with adsorption mechanisms dominated by micropore filling within heterogeneous porous structures. Although the calculated adsorption energy ($E = 59.199$ kJ/mol) indicates relatively strong adsorption interactions, the weak statistical agreement suggests that microporous filling is not the dominant mechanism governing NH_3–N adsorption. Instead, the adsorption process appears to occur primarily through surface interactions occurring on accessible mesostructured adsorption sites generated during CTAB assisted hydrothermal treatment.

The hybrid isotherm models, including Sips, Redlich–Peterson, and Fritz–Schlünder, also showed comparatively weaker fitting performance despite exhibiting moderate R^2 values ranging from 0.874 to 0.918. These models produced considerably larger error values, with χ^2 values approaching 3, RMSE values exceeding 1.19, and MAPE values above 7.5. The relatively high statistical deviations indicate that these complex hybrid models are less capable of accurately describing the experimental NH_3–N adsorption behavior. The Sips model generally describes adsorption systems combining heterogeneous multilayer adsorption characteristics, while the Redlich–Peterson and Fritz–Schlünder models are often applied to highly complex adsorption systems involving mixed adsorption mechanisms and broad energetic heterogeneity. However, the poorer fitting accuracy observed in this study suggests that NH_3–N adsorption on CTAB modified POFA does not primarily follow multilayer or highly heterogeneous adsorption pathways.

Overall, the isotherm analysis confirms that NH_3–N adsorption on CTAB modified POFA is predominantly governed by monolayer adsorption and specific surface interactions occurring at relatively homogeneous adsorption-active sites. The CTAB assisted hydrothermal modification not only improves pore accessibility and mesostructure formation but also alters the surface chemistry of POFA through the introduction of polar functional groups that enhance electrostatic attraction toward ammonia-containing species. These combined structural and chemical modifications contribute significantly to the improved adsorption performance observed in produced water treatment.

The isotherm analysis demonstrates that COD adsorption on modified POFA is controlled by a combination of monolayer and multilayer adsorption on a partially heterogeneous surface with a dominant chemisorption contribution. In contrast, NH_3–N adsorption follows predominantly Langmuir

behavior, indicating monolayer adsorption on relatively homogeneous active sites with strong surface affinity. These findings confirm that the surface characteristics of modified POFA, including its functional group density and hierarchical pore structure, play a decisive role in determining adsorption selectivity and removal efficiency for organic and nitrogenous pollutants in produced water. In this study, COD was used as a bulk indicator representing the overall organic content in produced water. Therefore, the adsorption behavior of individual organic compounds was not specifically evaluated. Further investigation using advanced analytical techniques such as GC–MS is recommended to provide deeper insight into pollutant-specific adsorption mechanisms.

4 Conclusion

The present study demonstrates that CTAB assisted hydrothermal modification successfully enhanced the adsorption performance of POFA for the simultaneous removal of COD and NH_3–N from produced water. The modification process improved the mesostructural characteristics of POFA by increasing pore accessibility, surface reactivity, and the distribution of active adsorption sites, thereby facilitating better interaction between pollutants and the adsorbent surface. The formation of mesoporous silica structures through CTAB directed hydrothermal treatment also reduced diffusion resistance and enhanced mass transfer of COD related organic compounds and NH_3–N species during adsorption. Adsorption performance was strongly influenced by operational parameters, with an optimum contact time of 180 min and an optimum adsorbent dosage of 0.3 g providing the highest overall removal efficiencies. At the optimum dosage of 0.3 g, COD removal reached 50.16 ± 1.03%, while NH_3–N removal achieved the highest value of 49.66 ± 0.99%. In addition, the optimum contact time of 180 min resulted in COD and NH_3–N removal efficiencies of approximately 53.98% and 38.34%, respectively. Equilibrium modeling indicates that COD adsorption is governed by a combination of monolayer and multilayer mechanisms on a partially heterogeneous surface, with evidence of dominant chemisorption interactions. In contrast, NH_3–N adsorption follows predominantly Langmuir-type behavior, confirming monolayer adsorption on relatively uniform active sites with higher affinity constants. The distinct adsorption characteristics between organic and nitrogenous pollutants highlight the importance of surface chemistry and active site distribution in controlling adsorption selectivity. Overall, the favorable adsorption performance and isotherm behavior confirm that modified POFA has strong potential as an effective adsorbent material for produced water remediation and offers promising prospects for sustainable wastewater treatment and industrial waste valorization applications.

Acknowledgements

This project is financially supported by the grant of Publication Acceleration Research Diponegoro (RAP UNDIP) No. 222-237/UN7·D2/PP/IV/2025. Special gratitude to the Institute for Research and Community Services, Diponegoro University (LPPM UNDIP) for the assistance during the completion of this project.

References

[1] Hidayah, M., Kusworo, T. D., Susanto, H. "Improving the Performance of Polysulfone-nano ZnO Membranes for Water Treatment in Oil Refinery with Modified UV Irradiation and Polyvinyl Alcohol", Periodica Polytechnica Chemical Engineering, 66(1), pp. 43–53, 2022. https://doi.org/10.3311/PPch.17029

[2] Aryanti, N., Kusworo, T. D., Oktiawan, W., Wardhani, D. H. "Performance of Ultrafiltration–Ozone Combined System for Produced Water Treatment", Periodica Polytechnica Chemical Engineering, 63(3), pp. 438–447, 2019. https://doi.org/10.3311/PPch.13491

[3] Farnan, J., Vanden Heuvel, J. P., Dorman, F. L., Warner, N. R., Burgos, W. D. "Toxicity and chemical composition of commercial road palliatives versus oil and gas produced waters", Environmental Pollution, 334, 122184, 2023. https://doi.org/10.1016/j.envpol.2023.122184

[4] Kusworo, T. D., Veda, A., Mafazan, R., Hasbullah, H., Bella Puspa, M. "Integrated Ozonation–Adsorption Pretreatment and Polyvinylidene Fluoride/Tungsten Based Polyoxometalate Photocatalytic Membrane for Produced Water Treatment", Periodica Polytechnica Chemical Engineering, 70(1), pp. 30–41, 2026. https://doi.org/10.3311/PPch.42654

[5] Zhao, D., Chen, L., Peng, M., Xue, B., Yao, Z., Huang, W., Wang, Z., Liu, J. "The complex influence of membrane roughness on colloidal fouling: A dialectical perspective", Journal of Membrane Science, 725, 124014, 2025. https://doi.org/10.1016/j.memsci.2025.124014

[6] Satyam, S., Patra, S. "Innovations and challenges in adsorption-based wastewater remediation: A comprehensive review", Heliyon, 10(9), e29573, 2024. https://doi.org/10.1016/j.heliyon.2024.e29573

[7] Fallah, Z., Roberts, E. P. L. "Combined adsorption/regeneration process for the removal of trace emulsified hydrocarbon contaminants", Chemosphere, 230, pp. 596–605, 2019. https://doi.org/10.1016/j.chemosphere.2019.04.224

[8] Vakili, M., Cagnetta, G., Deng, S., Wang, W., Gholami, Z., Gholami, F., Dastyar, W., Mojiri, A., Blaney, L. "Regeneration of exhausted adsorbents after PFAS adsorption: A critical review", Journal of Hazardous Materials, 471, 134429, 2024. https://doi.org/10.1016/j.jhazmat.2024.134429

[9] Mockshell, J., Villarino, M. E. J. "Agroecological Intensification: Potential and Limitations to Achieving Food Security and Sustainability", Encyclopedia of Food Security and Sustainability, 3, pp. 64–70, 2019. https://doi.org/10.1016/B978-0-08-100596-5.22211-7

[10] Hasnain, S. M. W. u., Farooqi, A. S., Victor Ayodele, B., Setiabudi, H. D., Farooqi, A. S., Alshareef, R. S., Abdullah, B. "Synthesis, characterization, and catalytic performance of Ni supported on sustainable POFA-derived SBA-15 for hydrogen-rich syngas from CO_2 reforming of methane", Journal of Industrial and Engineering Chemistry, 141, pp. 104–120, 2025. https://doi.org/10.1016/j.jiec.2024.06.021

[11] Mohamad Yusof, M. S., Othman, M. H. D., Abdul Wahab, R., Abu Samah, R., Kurniawan, T. A., Mustafa, A., Abdul Rahman, M., Jaafar, J., Ismail, A. F. "Effects of pre and post-ozonation on POFA hollow fibre ceramic adsorptive membrane for arsenic removal in water", Journal of the Taiwan Institute of Chemical Engineers, 110, pp. 100–111, 2020. https://doi.org/10.1016/j.jtice.2020.02.014

[12] Nessiani, R. K., Naseri, M., Ahmadzadeh, K., Erfani, H., Amesho, K. T. T. "Advanced simultaneous adsorption of heavy metals and organic dyes from aqueous solutions using CTAB-functionalized broccoli waste biochar: A sustainable approach for water remediation", Desalination and Water Treatment, 324, 101553, 2025. https://doi.org/10.1016/j.dwt.2025.101553

[13] Miao, R., Zeng, W., Gao, Q. "Hydrothermal synthesis of novel NiO nanoflowers assisted with CTAB and SDS respectively and their gas-sensing properties", Materials Letters, 186, pp. 175–177, 2017. https://doi.org/10.1016/j.matlet.2016.09.127

[14] Anas Al Tahan, M., Marwah, M., El-Zein, H., Al Tahan, S., Sanchez-Aranguren, L. "Exploring mesoporous silica microparticles in pharmaceutical sciences: Drug delivery and therapeutic insights", International Journal of Pharmaceutics, 678, 125656, 2025. https://doi.org/10.1016/j.ijpharm.2025.125656

[15] Mane, P. V., Rego, R. M., Yap, P. L., Losic, D., Kurkuri, M. D. "Unveiling cutting-edge advances in high surface area porous materials for the efficient removal of toxic metal ions from water", Progress in Materials Science, 146, 101314, 2024. https://doi.org/10.1016/j.pmatsci.2024.101314

[16] Tasnim, S., Rahman, M. E., Ahmadi, R. B. "Mechanical performance of modified cement paste made with micro-fine POFA in ammonium nitrate environment", Construction and Building Materials, 162, pp. 534–542, 2018. https://doi.org/10.1016/j.conbuildmat.2017.12.060

[17] Hanifa, N. H. E., Ismail, M., Ideris, A. "Utilization of palm oil fuel ash (POFA) as catalyst support for methane decomposition", Materials Today: Proceedings, 57, pp. 1136–1141, 2022. https://doi.org/10.1016/j.matpr.2021.10.007

[18] Aziz, A. S. A., Manaf, L. A., Man, H. C., Kumar, N. S. "Equilibrium studies and dynamic behavior of cadmium adsorption by palm oil boiler mill fly ash (POFA) as a natural low-cost adsorbent", Desalination and Water Treatment, 54(7), pp. 1956–1968, 2015. https://doi.org/10.1080/19443994.2014.891466

[19] Lei, X., Liu, B., Di, C., Wei, Z., Deng, P., Chen, Z. "Molecular interactions of surfactants with other chemicals in chemical flooding processes: A comprehensive review on molecular dynamics simulation studies", Advances in Colloid and Interface Science, 341, 103498, 2025. https://doi.org/10.1016/j.cis.2025.103498

[20] Nasirpouri, F., Fallah, S., Ahmadpour, G., Moslehifard, E., Samardak, A. Y., Samardak, V. Y., Ognev, A. V., Samardak, A. S. !Microstructure, ion adsorption and magnetic behavior of mesoporous γ-Fe_2O_3 ferrite nanoparticles", RSC Advances, 13(36), pp. 25140–25158, 2023. https://doi.org/10.1039/d3ra01663c

[21] Gundanna, S. K., Mitra, A., Bhatta, L. K. G., Bhatta, U. M. "Effect of thermal treatment on the surface/interfacial behaviour of Au@SiO_2 nanoparticles in the presence of CTAB surfactant molecules", Powder Technology, 381, pp. 503–508, 2021. https://doi.org/10.1016/j.powtec.2020.12.010

[22] Olivia, M., Asmanovita, R., Sinuhaji, I. J., Putri, W. R., Sitompul, I. R., Utama, P. S., Supit, S. W. M. "Properties of blended Palm Oil Fuel Ash (POFA) concrete using additive micro silica exposed to organic peat water environment", Cleaner Waste Systems, 12, 100414, 2025. https://doi.org/10.1016/j.clwas.2025.100414

[23] Hu, H., Cai, T., Tong, Y., Wang, J., Zhou, L., …, Xing, W. "Stepwise construction of Si–O–C and Si–C collaborative interfaces for highly stable silicon anodes", Energy Storage Materials, 84, 104818, 2026. https://doi.org/10.1016/j.ensm.2025.104818

[24] Yang, J., Xiang, Y., Xu, J., Shi, C., Pan, L., Zhang, X., Zou, J.-J. "Ti/MCM-41 with highly active Si-O-Ti structures for efficient extraction and oxidative desulfurization of fuel oil", Chemical Engineering Science, 320, 122613, 2026. https://doi.org/10.1016/j.ces.2025.122613

[25] Kim, B., Devarayapalli, K. C., Lee, D. S. "CTAB-engineered $Ti_3C_2T_x$-derived TiO_2 for mechanistically robust and efficient photocatalytic reduction of perrhenate under solar irradiation", Journal of Water Process Engineering, 83, 109722, 2026. https://doi.org/10.1016/j.jwpe.2026.109722

[26] Mittal, R., Patar, S., Sharma, A., Bhateria, R., Kumar Bhardwaj, A., Kashyap, R., Bhukal, S. "Surface modified novel synthesis of *Spirulina* assisted mesoporous TiO_2@CTAB nanocomposite employed for efficient removal of chromium (VI) in wastewater", Applied Surface Science, 679, 161309, 2025. https://doi.org/10.1016/j.apsusc.2024.161309

[27] Shan, Y., Chen, C., Liang, Y., Chen, Y., Wu, Y., …, Cheng, J. "CTAB optimized TiO_2@Fe_3S_4 photocatalyst for efficient separation and homogeneous degradation of organic pollutants", Journal of Alloys and Compounds, 1031, 181017, 2025. https://doi.org/10.1016/j.jallcom.2025.181017

[28] Lyn, C. W., Bashir, M. J. K., Wong, L. Y., Lim, J. W., Sethupathi, S., Ng, C. A. "Ancillary palm oil fuel ash (POFA) in sequencing batch reactor for enhancing recalcitrant pollutants removal from domestic wastewater", Chemosphere, 265, 129050, 2021. https://doi.org/10.1016/j.chemosphere.2020.129050

[29] Jafarlou, A., Javadi, A., Miller, R., Eckert, K. "Dynamics of adsorption of CTAB-Silica nanoparticle complexes: New experiments and modeling approach", Colloids and Surfaces A: Physicochemical and Engineering Aspects, 629, 127448, 2021. https://doi.org/10.1016/j.colsurfa.2021.127448

[30] Gao, H., Zhou, Y., Sheng, X., Zhao, S., Zhang, C., Zhang, M. "Synthesis of core-shell and hollow structured dual-mesoporous silica templated by alkoxysilyl-functionalized ionic liquids and CTAB", Materials Letters, 211, pp. 126–129, 2018. https://doi.org/10.1016/j.matlet.2017.09.067

[31] Haghighatzadeh, A., Mazinani, B., Shokouhimehr, M., Samiee, L. "Preparation of mesoporous TiO_2–SiO_2 by ultrasonic impregnation method and effect of its calcination temperature on photocatalytic activity", Desalination and Water Treatment, 92, pp. 145–151, 2017. https://doi.org/10.5004/dwt.2017.21481

[32] Modwi, A., Khezami, L., Ghoniem, M. G., Nguyen-Tri, P., Baaloudj, O., Guesmi, A., AlGethami, F. K., Amer, M. S., Assadi, A. A. "Superior removal of dyes by mesoporous MgO/g-C_3N_4 fabricated through ultrasound method: Adsorption mechanism and process modeling", Environmental Research, 205, 112543, 2022. https://doi.org/10.1016/j.envres.2021.112543

[33] Yeh, S.-W., Ko, H.-H., Chiang, H.-M., Chen, Y.-L., Lee, J.-H., Wen, C.-M., Wang, M.-C. "Characteristics and properties of a novel in situ method of synthesizing mesoporous TiO_2 nanopowders by a simple coprecipitation process without adding surfactant", Journal of Alloys and Compounds, 613, pp. 107–116, 2014. https://doi.org/10.1016/j.jallcom.2014.05.227

[34] Thomas Hendges, L., Gómez González, S. Y., Weschenfelder, S. E., de Fatima Rodrigues da Cunha, M., da Silva, A., Prazeres Mazur, L., Alcantara Marinho, B., Ulson de Souza, A. A., A. Guelli Ulson de Souza, S. M. "Reducing oil and grease on-site in real offshore oilfield-produced water through feasible adsorption-desorption cycling", Journal of Water Process Engineering, 66, 105962, 2024. https://doi.org/10.1016/j.jwpe.2024.105962

[35] Kusworo, T. D., Seng, K. S., Arutanti, O., Puspa, M. B., Hasbullah, H., Dalanta, F. "Visible-light-driven Z-scheme Ag-doped WO_3/$BiVO_4$ ternary nanocomposite with a synergistic adsorption-photocatalytic feature for enhanced oil field produced water treatment", Journal of Water Process Engineering, 81, 109250, 2026. https://doi.org/10.1016/j.jwpe.2025.109250

[36] Kusworo, T. D., Puspa, M. B., Kumoro, A. C., Sutapa, I. D. A., Utomo, D. P. "Novel photosensitive La@TiO_2 nanocomposite: A breakthrough in visible-light photocatalysis for oil field water treatment", Case Studies in Chemical and Environmental Engineering, 10, 100884, 2024. https://doi.org/10.1016/j.cscee.2024.100884

[37] Ewis, D., Ba-Abbad, M. M., Benamor, A., El-Naas, M. H. "Adsorption of organic water pollutants by clays and clay minerals composites: A comprehensive review", Applied Clay Science, 229, 106686, 2022. https://doi.org/10.1016/j.clay.2022.106686

[38] Cao, S., Zhu, R., Wu, D., Su, H., Liu, Z., Chen, Z. "How hydrogen bonding and π–π interactions synergistically facilitate mephedrone adsorption by bio-sorbent: An in-depth microscopic scale interpretation", Environmental Pollution, 342, 123044, 2024. https://doi.org/10.1016/j.envpol.2023.123044

[39] Han, B., Butterly, C., Zhang, W., He, J., Chen, D. "Adsorbent materials for ammonium and ammonia removal: A review", Journal of Cleaner Production, 283, 124611, 2021. https://doi.org/10.1016/j.jclepro.2020.124611

[40] Singh, M., Hakimabadi, S. G., Van Geel, P. J., Carey, G. R., Pham, A. L.-T. "Modified competitive Langmuir model for prediction of multispecies PFAS competitive adsorption equilibria on colloidal activated carbon", Separation and Purification Technology, 345, 127368, 2024. https://doi.org/10.1016/j.seppur.2024.127368

[41] Nnadozie, E. C., Ajibade, P. A. "Data for experimental and calculated values of the adsorption of Pb(II) and Cr(VI) on APTES functionalized magnetite biochar using Langmuir, Freundlich and Temkin equations", Data in Brief, 32, 106292, 2020. https://doi.org/10.1016/j.dib.2020.106292

[42] Wortmann, F. J., Hardie, K., Schellenberg, N., Jones, C., Wortmann, G., Schulze zur Wiesche, E. "pH-equilibration of human hair: Kinetics and pH-dependence of the partition ratios for H^+ − and OH^- -ions based on a Freundlich isotherm", Biophysical Chemistry, 297, 107010, 2023. https://doi.org/10.1016/j.bpc.2023.107010

[43] Abbas, R. F., Hassan, M. J. M., Rheima, A. M. "Adsorption of fast green dye onto Fe_3O_4 MNPs and GO/Fe_3O_4 MNPs synthesized by photo-irradiation method: Isotherms, thermodynamics, kinetics, and reuse studies", Sustainable Chemistry for the Environment, 6, 100104, 2024. https://doi.org/10.1016/j.scenv.2024.100104

[44] Fakhri, A., Behrouz, S. "Comparison studies of adsorption properties of MgO nanoparticles and ZnO–MgO nanocomposites for linezolid antibiotic removal from aqueous solution using response surface methodology", Process Safety and Environmental Protection, 94, pp. 37–43, 2015. https://doi.org/10.1016/j.psep.2014.12.007

[45] Tadayoni, N. S., Dinari, M. "Novel bio-adsorbent of alginate/HTC hydrochar & alginate/HTH hydrochar composite beads for removal of basic blue 9 from water", Carbohydrate Polymer Technologies and Applications, 10, 100856, 2025. https://doi.org/10.1016/j.carpta.2025.100856